

## **General Disclaimer**

### **One or more of the Following Statements may affect this Document**

- This document has been reproduced from the best copy furnished by the organizational source. It is being released in the interest of making available as much information as possible.
- This document may contain data, which exceeds the sheet parameters. It was furnished in this condition by the organizational source and is the best copy available.
- This document may contain tone-on-tone or color graphs, charts and/or pictures, which have been reproduced in black and white.
- This document is paginated as submitted by the original source.
- Portions of this document are not fully legible due to the historical nature of some of the material. However, it is the best reproduction available from the original submission.

**NASA TECHNICAL  
MEMORANDUM**

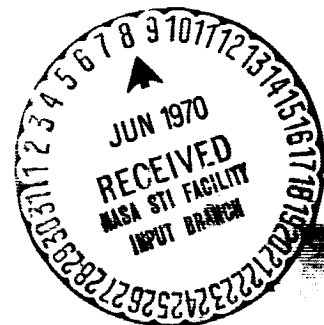
NASA TM X-52753

NASA TM X-52753

**EXPERIMENTAL LOAD CAPACITY AND POWER LOSS OF  
HERRINGBONE GROOVED GAS LUBRICATED JOURNAL BEARINGS**

by Robert E. Cunningham, David P. Fleming, and William J. Anderson  
Lewis Research Center  
Cleveland, Ohio

TECHNICAL PAPER proposed for presentation at  
1970 Spring Lubrication Symposium sponsored by  
the American Society of Mechanical Engineers  
Detroit, Michigan, May 25-27, 1970



FACILITY FORM 602

N70-38550  
(ACCESSION NUMBER)

19  
(PAGES)

TMX 52753  
(NASA CR OR TMX OR AD NUMBER)

1  
(THRU)

15  
(CODE)

15  
(CATEGORY)

**EXPERIMENTAL LOAD CAPACITY AND POWER LOSS OF HERRINGBONE  
GROOVED GAS LUBRICATED JOURNAL BEARINGS**

by Robert E. Cunningham, David P. Fleming, and William J. Anderson

Lewis Research Center  
Cleveland, Ohio

**TECHNICAL PAPER** proposed for presentation at  
1970 Spring Lubrication Symposium  
sponsored by the American Society of Mechanical Engineers  
Detroit, Michigan, May 25-27, 1970

**NATIONAL AERONAUTICS AND SPACE ADMINISTRATION**

## EXPERIMENTAL LOAD CAPACITY AND POWER LOSS OF HERRINGBONE

### GROOVED GAS LUBRICATED JOURNAL BEARINGS

by Robert E. Cunningham, David P. Fleming and William J. Anderson

Lewis Research Center  
National Aeronautics and Space Administration  
Cleveland, Ohio

#### ABSTRACT

Load capacity, attitude angle, and power loss were determined for  $\frac{1}{2}$  inch diameter herringbone grooved journal bearings operating in air to speeds of 60 000 rpm. Results showed that groove-to-ridge-clearance ratios of 2.0 to 2.4 give a greater load capacity than do ratios outside this optimum range. Agreement with a small-eccentricity pressure perturbation theory was good for groove-to-ridge-clearance ratios in the optimum range. Power loss, relative to that calculated for a plain bearing of the same dimensions, did not vary widely for the range of geometric variables used. Relative power loss increased with speed and was generally higher than for a plain bearing.

#### INTRODUCTION

Turbomachinery used in space power systems must be compact and light weight. In addition, since energy sources for these applications are usually limited, internal losses must be minimized. Process fluid lubrication can help to achieve these goals. Components such as oil sumps and pumps, seals, and oil scavenging and separating systems are eliminated. Since the viscosity of the working fluid (usually a gas or liquid metal) is less than that of normal lubricating oils, friction power losses in the bearings can also be reduced. This is especially true when the working fluid is a gas, as in the Brayton cycle machinery currently under development (Ref. 1).

Self-excited instability is a severe problem in gas-lubricated bearings. At high speeds and low loads the bearing journal may precess about its steady state position. The frequency of this precession, for a self-acting bearing, is usually about one-half of the rotational frequency; thus, the phenomenon has become known as half-frequency whirl. A major part of the research in gas-lubricated bearings has been directed toward development of bearing configurations that will operate stably when the load is small or zero.

One design which has operated stably at high speeds, even when unloaded, is the herringbone-grooved bearing (Refs. 2 and 3). Shallow

helical grooves are cut in either the journal or the bearing to create an inward pumping viscous pump. The pressure field created is similar to that in an externally pressurized bearing. In the herringbone bearing, however, the pressure increases continuously with increasing speed.

The analysis of reference 4 predicts that the load capacity of a herringbone bearing also increases continuously with speed. At moderate and high compressibility numbers, the herringbone bearing's load capacity surpasses that of a plain bearing. These findings seem to be borne out by the experimental work of reference 3, which tested one particular groove geometry to a maximum compressibility number of 16.

In order to assure stable operation, clearances in a herringbone bearing must be kept small, approximately  $0.5 \times 10^{-3}$  inch radial clearance per inch of shaft radius. Thus, power loss in these bearings could well be higher than in other bearing types operating with larger clearances. Because of the nonuniform clearance created by the herringbone grooves, calculation of the friction power loss is not possible with present techniques, and experimental measurements are necessary.

The objectives of the investigation were (1) to measure the load capacity, attitude angle, and friction power loss in herringbone-grooved bearings having various groove angles and widths; (2) to compare the load capacity and attitude angles with those obtained from the theory of references 4; and (3) to compare the power loss with the calculated values for a smooth journal bearing and with available data for other bearing types.

#### SYMBOLS

B	coefficient
C	radial clearance, in.
D	bearing (rotor) dia. in.
E	elastic modulus, lb/in. <sup>2</sup>
e	rotor eccentricity, in.
H	ratio of groove clearance to ridge clearance = $1 + \delta/C$
I	rotor polar moment of inertia, in lb sec <sup>2</sup>
L	bearing length, in.
L <sub>1</sub>	length of grooves, in.
N	rotor speed, rpm
n	number of grooves
P	power loss in herringbone bearing, watts
P <sub>p</sub>	power loss in plain bearing, watts
p <sub>a</sub> <sup>p</sup>	ambient pressure, lb/in. <sup>2</sup>
R <sub>a</sub>	bearing radius, in.
t	time, sec

$W$	applied load per bearing, lb
$\bar{W}$	dimensionless load, $W/p_aLD$
$\alpha$	ratio of groove width to width of groove-ridge pair, $a_g/(a_g + a_r)$
$\beta$	groove helix angle, deg
$\delta$	groove depth, in.
$\epsilon$	eccentricity ratio, $e/C$
$\Lambda$	bearing compressibility number $6\mu\omega R^2/p_a C^2$
$\mu$	lubricant viscosity, lb sec/in. <sup>2</sup>
$\nu$	Poisson's ratio
$\rho$	rotor density, lb sec <sup>2</sup> /in.
$\phi$	bearing attitude angle, deg
$\omega$	rotor speed, rad/sec

## Subscript:

0 zero speed

## APPARATUS

The basic experimental apparatus is identical to that used in reference 2 and is described fully therein. It consists of a steel rotor mounted in two smooth bronze bushings which have been in-line bored (Fig. 1). The rotor is  $1\frac{1}{2}$  inches in diameter and  $12\frac{1}{4}$  inches long, and has two herringbone-groove patterns on its surface (Fig. 2). Each of the bronze bushings is  $1\frac{1}{2}$  inches long; thus the length-to-diameter ratio is 1. Externally pressurized thrust bearings position the rotor axially.

The apparatus was oriented with the rotor axis vertical for the power loss measurements, in order to have concentric operation. For the load capacity measurements, the rotor was horizontal. Steady radial loads were applied to the rotor by an externally pressurized load shoe (Fig. 1). A spherical pivot couples the load shoe to the shaft of a rolling diaphragm air cylinder.

The rotor is driven by an impulse turbine which consists of a number of buckets cut into the upper end of the rotor and a nozzle ring surrounding the rotor. A magnetic pickup adjacent to the turbine buckets is connected to a digital counter to measure rotor speed.

Two orthogonally oriented capacitance distance probes are mounted outboard of each bearing. They were used to measure the displacement of the rotor under load, and also the assembled clearance of the rotor in the bearings. A fifth capacitance probe, flush with the thrust bearings surface, was used to monitor thrust bearing clearance for power loss measurements.

Eight different herringbone-grooved rotors were used, with three sets of bronze bearings. The characteristics of the grooves and assembled bearings are listed in table I. All rotors were not run in all sets of bearings. Those combinations that were used are indicated by clearance values appearing in the "turbine end" column for load capacity tests, and in the "average" column for power loss tests.

#### PROCEDURE

Load capacity measurements. - The rotor was accelerated to the desired test speed, and the loads adjusted so the applied upward force just balanced the weight of the rotor. The capacitance probe outputs were recorded for this zero-net-load or concentric position. Load was then applied to the test bearings by increasing the pressure to the diaphragm air cylinder in increments of 1 or 2 psi. At each load increment, probe outputs were again recorded. After maximum load was reached, the bearings were unloaded. The speed was then increased to a new value and the foregoing procedure repeated.

Power loss measurements. - After maximum speed was reached, the turbine air was shut off and the rotor allowed to coast down in speed. During the coast period, readings of the digital speed counter were recorded at regular time intervals, electronically determined by the counter. The length of the interval was subsequently calculated by recording the total elapsed time of the experimental run, and dividing this time by the number of speed readings. The test was stopped when the rotor speed had decayed to approximately 1000 revolutions per minute. With the time interval between speed readings known, a time value could be assigned to each speed reading. These pairs of values defined a speed-time function.

The torque acting on the rotor is the product of rotor polar moment of inertia and rotor acceleration.

$$T = -I \frac{d\omega}{dt} \quad (1)$$

Since numerical differentiation is inherently inaccurate, rotor acceleration was determined by fitting an analytical function to the speed-time data and differentiating this function analytically. It proved convenient to consider time as a function of rotor speed, rather than the usual inverse relation. The function to be fitted to the experimental data was chosen as

$$t = B_1 + B_2 \ln N + B_3 N + B_4 N^2 \quad (2)$$

in which  $N$  is the rotor speed in revolutions per minute. The terms in  $N$  and  $N^2$  allow for the behavior of the herringbone bearing being different than that of a plain bearing. The coefficients  $B_1$  through  $B_4$  were determined to provide a least-squared-error fit to the particular experimental data being examined. Equation (2) may be differentiated to give the reciprocal of the acceleration. Power loss, the product of torque and speed, is then given by

$$P = - \frac{\pi^2}{900} \frac{IN}{dt/dN} \quad (3)$$

Power loss in the thrust bearings was calculated and subtracted from the measured power loss to obtain the net power loss in the herringbone bearings. More details on the handling of the data are in reference 5.

The entire data reduction process of calculating herringbone clearances from capacitance probe readings, fitting the least-squares curve to speed decay data, and computing power loss values was handled by a digital computer.

## RESULTS AND DISCUSSION

Experimental results obtained with eight herringbone-grooved rotors are plotted in figures 3 through 10. These rotors, whose groove characteristics are listed in table I were operated in ambient air to a maximum compressibility number of 45. Maximum speed was 60 000 rpm.

Load capacity and attitude angle. - Steady loads were varied up to 20.8 lb/in.<sup>2</sup> of projected bearing area. All steady load data is plotted for the turbine and bearing. Dimensionless load as a function of eccentricity ratio is plotted in figure 3. These experimental curves have a shape characteristic of self-acting bearings in that the load capacity increases sharply with increasing eccentricity ratio. The straight dashed lines are predictions from the small eccentricity analysis of reference 4. Agreement between theory and experiment is only fair. At eccentricity ratios of 0.3 and less, where the theory is applicable, the experimentally determined load capacity is less than predicted at low compressibility numbers, while the opposite is true at the higher compressibility numbers. Additional load-deflection data for other groove geometries are plotted in reference 6.

Dimensionless load as a function of compressibility number is plotted in figures 4(a) and (b) for five different herringbone grooved rotors. Basically, this shows how load capacity varies with speed. The experimental curves are cross plots of the load-deflection data. Also plotted are minimum and maximum theoretical curves for the geometries used.

Figure 4(a), for an eccentricity ratio of 0.3, shows that the analytical results generally overestimate the load capacity. However, the load capacity of rotor A-1 was greater than the prediction above a compressibility number of about 12. It appears that the load capacities of rotors A-5 and A-7 might also exceed the theoretical values if they could be run at higher compressibility numbers.

The curves for rotors A-1, A-2, and A-7 are quite close together, whereas rotors A-3 (low clearance) and A-5 had considerably less load capacity. The ratio of groove clearance to land clearance,  $H$ , varied from 2.0 to 2.4 for the 3 rotors having the higher load capacity, but  $H$  was 2.7 for both rotor A-3 (low clearance) and A-5 (table I). This corresponds with the analysis of reference 4, which shows that, at very low compressibility numbers the load capacity decreases with increasing groove depth ratio, while at a compressibility number of 20, load capacity peaks at a value of  $H$  near 2. Groove depth ratios much less than 2 were not used in these experiments because of stability considerations.

If only rotors with groove-to-land-clearance ratios in the range 2.0 to 2.4 are considered, figure 4(a) shows that agreement with theory is quite good out to compressibility numbers of about 17.

Figure 4(b), for an eccentricity ratio of 0.5, leads to essentially the same conclusions drawn from figure 4(a). Again, rotor A-1 is the only one exceeding the theoretical prediction, and only at higher compressibility numbers. A curve for rotor A-3 (high clearance,  $H = 1.9$ ) appears here slightly below the other curves for rotors A-1, A-2, and A-7. The curve for rotor A-3 (low clearance,  $H = 2.7$ ) with its large groove depth ratio, is again significantly below the others. (Rotor A-5, which also had  $H = 2.7$ , was not operated out to  $\epsilon = 0.5$ ).

The data plotted in figure 5 are those of the journal attitude eccentricity loci in polar coordinates. The most significant feature in this plot is the negative attitude angles observed at the highest compressibility numbers. These negative attitude angles were predicted by the analysis of reference 4. Attitude angles generally decrease as eccentricity increases. This is not, of course, predicted by the pressure perturbation analysis of reference 4, but is expected behavior in journal bearings. This is illustrated by the solid curve in figure 5; it represents the theoretical attitude-eccentricity locus for a plain

journal bearing (ref. 7).

Figure 6 shows experimental attitude angles as a function of compressibility number for an eccentricity ratio of 0.3. Also shown are the minimum and maximum attitude angles predicted by the theory of reference 4. Measured attitude angles are generally higher than predicted. Exceptions are for rotors A-1 and A-7 at the higher compressibilities of their operating range. The theory predicts negative attitude angles at high compressibility numbers; these were observed for three of the rotors tested.

#### Power Loss

Figure 7 shows a typical set of data points for the herringbone bearing speed decay, and the least-squares curve fitted. The curve fits the data very well, indicating that the herringbone bearing behaves sufficiently like a plain bearing so that the two correction terms  $B_3N$  and  $B_4N^2$  of equation (2) are adequate.

With the speed-time function known (eq. (2)), power loss was calculated by equation (3). The solid curve of figure 8 illustrates the power loss as a function of speed for the herringbone-grooved bearing whose speed-time trace appears in figure 7.

For an ungrooved full circular journal bearing, the power loss is easily calculated to be

$$P_p = 2\pi\mu\omega^2 R^3 L / C \quad (5)$$

This formula was used to calculate the power loss in a plain bearing having the same dimensions and clearance as the herringbone bearing of figure 8. The result appears as the dot-dash curve of figure 8 (because a plain bearing is inherently unstable, it was not possible to measure its power loss experimentally). The bearing clearance at zero speed was used in this calculation. Because of centrifugal force, the rotor diameter increases with increasing speed; thus the bearing clearance decreases. The increase in diameter for a solid rotor may be calculated by (ref. 8)

$$\Delta D = \frac{\rho \omega^2 R^3 (1 - \nu)}{2E} \quad (6)$$

in which  $\nu$  is Poisson's ratio for the rotor,  $\rho$  the rotor density, and  $E$  the elastic modulus. The dashed curve of figure 8 shows the power loss of a plain bearing when the decrease in clearance is taken into account.

From equation (5) it is evident that power loss in a plain journal bearing depends rather strongly on clearance. A comparison of power losses for different herringbone bearings would have little meaning, therefore, unless they could be normalized with respect to clearance. A convenient normalizing function is the power loss in a plain bearing which has the same dimensions and clearance as the herringbone bearing under study. The power loss relative to a plain bearing should not be looked at as a measure of the advantage or disadvantage of using a herringbone bearing rather than a plain bearing, but only as a convenient dimensionless representation. A plain bearing usually cannot be used at all because of its inherent instability.

The relative power loss  $P/P_p$  has been plotted against speed in figure 9 ( $P$  is the herringbone bearing power loss, and  $P_p$  the power loss in an equivalent plain bearing calculated by equation (5)). The rotor designation and zero speed clearance are indicated on each curve. The plain bearing power loss was calculated with a clearance which was corrected for centrifugal growth of the rotor (eq. (6)).

The most striking features of this figure are the close grouping of the curves and the fact that the relative power loss increases with speed at nearly the same rate for all of the configurations tested. The slope of the curves is approximately  $1.2 \times 10^{-5}/\text{rpm}$ . Several of the curves flatten out at high speed. Figure 10 compares relative power losses among the various herringbone bearings tested using the bearing compressibility number  $\Lambda$  as a speed parameter.

$$\Lambda = \frac{6\mu\omega}{P_a} \left(\frac{R}{C}\right)^2 \quad (7)$$

This is the quantity that is most commonly used to characterize speed in gas lubrication work. The compressibility number was calculated using the centrifugal growth corrected clearance. The curves are again grouped closely together, though not as closely as in figure 9. The leveling off of the curves at high speed is somewhat more pronounced than in figure 9, and the curves appear to radiate from a common point, rather than being parallel. There is a fairly consistent trend of

higher relative power loss with increasing clearance. This trend can be explained by examination of the definition of  $\Lambda$ , equation (7). Since all of the factors appearing in  $\Lambda$ , except speed and clearance, remained constant throughout the work discussed herein, it follows that

$\Lambda$  is proportional to  $\text{rpm}/C^2$ . A larger clearance results in a lower value of  $\Lambda$  and a curve from figure 9 is shifted to the left when it is replotted in figure 10. All of the curves have a positive slope, thus, moving a curve to the left will make it appear higher.

The positive slope of the curves of figures 9 and 10 can be explained as follows. The clearance in a herringbone-grooved bearing is conventionally expressed as the clearance over the ridges. In the grooves, the clearance is larger than this by the depth of the groove. The mean clearance is between these two values.

At low speeds, the lubricant flow, due to rotation of the bearing, will be largely as given by potential theory. This is illustrated by the plot of streamlines in figure 11(a). Under this condition, the average transverse velocity gradient in the groove is less than that over the ridges, and the power loss is less than that for a plain bearing whose clearance equals the ridge clearance.

As the speed increases, laminar eddies develop, and there is a circulation of fluid within the groove, approximately as depicted in figure 11(b). The effect of this circulation is to increase the power loss over that of the potential flow case. It is reasonable to expect this increase to approach a limit as the laminar eddies become "fully developed"; this explains the leveling off of the curves of figures 9 and 10. True turbulence is not expected to occur in gas-lubricated bearings. When the groove clearance and maximum pressure in the bearing (calculated according to Ref. 4) are used in the calculation of a Reynolds number, the largest attained in the experimental work was 440 for rotor B<sub>1</sub> ( $C_0 = 0.49$  mils). This is the maximum Reynolds number and is far below the transition (1730 for this configuration, Ref. 9).

Some general observations can be made from figures 9 and 10. The spread of the curves is fairly small in each of the figures; the greatest is about 25 percent. The spread is least when the dimensional speed in revolutions per minute is used as the independent variables (Fig. 9) rather than the dimensionless parameter  $\Lambda$  (Fig. 10). In figure 9 the variation among curves at 50 000 rpm is only 15 percent. On both figures, rotors A6 and A7, with narrower grooves than the others ( $\alpha = 0.3$  against 0.5), show generally higher power loss. Among the other rotors, there appears to be a slight trend toward increasing power loss with increasing groove angle  $\beta$ . The depth of the grooves does not seem to affect power loss. The one fully grooved rotor (B1)

seems to have a lower power loss than the other, partially grooved rotors. On the whole, differences among the various herringbone configurations are slight.

Perhaps the most widely used gas journal bearing in prototype turbomachinery is the tilting pad bearing. If herringbone bearings are considered as replacements for tilting pad bearings, knowledge of the respective power losses would be useful. Reference 1 estimates the power loss for two 3-pad journal bearings as 120 watts at 38 500 rpm. These bearings have a diameter of 1.75 inches and a length/diameter ratio of 0.75 (Ref. 10). The lubricant gas was argon. The present test bearings have a diameter of 1.5 inches, a length-to-diameter ratio of 1, and operate in air. In order to have a basis for comparison, it will be assumed that equation (5) applies to the tilting pad bearing, except for a proportionality factor. It will be further assumed that in reducing the size of the bearing the ratio of radius to clearance remains constant. Then, for operation at constant speed,

$$P \approx \mu R^3 \frac{L}{D} \quad (8)$$

The power loss in two tilting pad bearings operating in air and having the same dimensions as the present herringbone bearings would then be 83 watts (viscosity data taken from Ref. 11). The power loss in the experimental herringbone bearing at 38 500 rpm varied from 89 to 138 watts; the average was 116 watts. Thus, the herringbone bearing power loss is, on the average, 1.4 times that in the example tilting pad bearing. Whether the advantages of the herringbone bearing (fewer parts, smaller bearing envelope, higher load capacity) compensate for the increased power loss must be evaluated for the particular application. Because of its increasing load capacity at higher speeds, it may be possible to use a smaller herringbone bearing than tilting pad bearing in a given application; therefore, it is possible that power loss could be reduced by using herringbone bearings.

#### SUMMARY OF RESULTS

Experiments were conducted to determine the load capacity, attitude angle, and power loss in herringbone-grooved journal bearings. The bearings were operated in air to speeds of 60 000 rpm; maximum compressibility number was 45. The following results were obtained:

1. An average groove-to-ridge clearance ratio  $H$  of 2.0 to 2.4 showed greater load capacity than ratios greater or less than this opt-

imum range.

2. Load capacity increased at a rate greater than linear with increasing eccentricity ratio. The load capacity of rotors with groove-to-ridge-clearance ratios in the optimum range agreed well with theory at low to moderate compressibility numbers. At high compressibility numbers and eccentricities, load capacity sometimes exceeded theoretical.

3. Negative attitude angles, predicted by theory, were observed with three of the rotors at high speeds.

4. Within the range of geometric variables used, power loss, relative to that calculated for a plain bearing of the same dimensions, did not vary widely. Power loss appeared to increase slightly with increasing groove angle and decreasing groove width. The one fully grooved rotor tested had generally lower power loss than the partially grooved rotors. Groove depth did not seem to influence power loss.

5. Relative power loss increased with speed. Except at low speeds, power loss was greater in the herringbone bearings than in equivalent size plain bearings. Power loss increased with speed at nearly the same rate in all of the herringbone bearings used.

#### REFERENCES

1. R. Y. Wong, W. L. Stewart, and H. E. Rohlik, "Pivoted-Pad Journal Gas Bearing Performance in Exploratory Operation in Brayton Cycle Turbocompressor", Journal of Lubrication Technology, vol. 90, no. 4, October 1968, pp. 687-696.
2. R. E. Cunningham, D. P. Fleming, and W. J. Anderson, "Experimental Stability Studies of the Herringbone-Grooved Gas-Lubricated Journal Bearing", Journal of Lubrication Technology, vol. 91, no. 1 January 1969, pp. 52-59.
3. S. B. Malanoski, "Experiments on an Ultrastable Gas Journal Bearing", Journal of Lubrication Technology, vol. 89, no. 4, October 1967, pp. 433-438.
4. J. H. Vohr and C. L. Chow, "Characteristics of Herringbone-Grooved, Gas-Lubricated Journal Bearings", Journal of Basic Engineering, vol. 87, no. 3, September 1965, pp. 568-578.
5. D. P. Fleming, R. E. Cunningham, and W. J. Anderson, "Experiments on Power Loss in Herringbone-Groove, Gas-Lubricated Journal Bearings", NASA TN D-5224, 1969.

6. R. E. Cunningham, D. P. Fleming, and W. J. Anderson, "Experiments on the Steady-State Characteristics of Herringbone-Grooved Air-Lubricated Journal Bearings", NASA TN D-5386, 1969.
7. A. A. Raimondi, "A Numerical Solution for the Gas Lubricated Full Journal Bearing of Finite Length", ASLE Transactions, vol. 4, no. 1, April, 1961, pp. 131-155.
8. S. Timoshenko, Theory of Elasticity, McGraw-Hill Book Co., Inc., New York, 1934, pp. 63, 68.
9. G. I. Taylor, "Stability of a Viscous Liquid Contained Between Two Rotating Cylinders", Philosophical Transactions of the Royal Society of London, series A, vol. 223, 1923, pp. 289-343.
10. Anon, "Design and Fabrication of a High-Performance Brayton Cycle Radial-Flow Gas Generator", NASA CR-706, 1967
11. C. D. Hodgman, ed., Handbook of Chemistry and Physics, 42nd ed., Chemical Rubber Publishing Co., Cleveland, Ohio, 1961.

TABLE I. - CHARACTERISTICS OF HERRINGBONE-GROOVED ROTORS.  $L/D = 1$ ,  $L_1/L = 0.6$

Rotor	Groove angle B, deg	Groove width/ (groove width and ridge width), $\alpha$	Number of grooves, n	Groove depth, mills		Zero-speed radial clearance, mills		Ratio of groove clearance to ridge clearance, H	
				Turbine end	Average	Turbine end	Average	Turbine end	Average
A1	30	0.5	20	0.58	0.56	0.40	0.41	2.4	2.4
A1	30	.5	20	.58	.56	----	.56	----	2.0
A2	35	.5	20	.64	.64	.47	.49	2.4	2.3
A2	35	.5	20	.64	.64	----	.67	----	2.0
A3	35	.5	23	.54	.59	.32	----	2.7	----
A3	35	.5	23	.54	.59	----	.42	----	2.4
A3	35	.5	23	.54	.59	.63	.63	1.9	1.9
A4	40	.5	23	----	.65	----	.41	----	2.6
A5	40	.5	28	.71	.75	.41	----	2.7	----
A5	40	.5	28	.71	.75	----	.51	----	2.5
A5	40	.5	28	.71	.75	----	.71	----	2.1
A6	35	.3	36	----	.36	----	.48	----	1.8
A7	40	.3	40	.54	.57	.52	.50	2.0	2.1
B1 <sup>a</sup>	30	.5	20	----	.50	----	.49	----	2.0

<sup>a</sup>Fully grooved,  $L_1/L = 1$ .

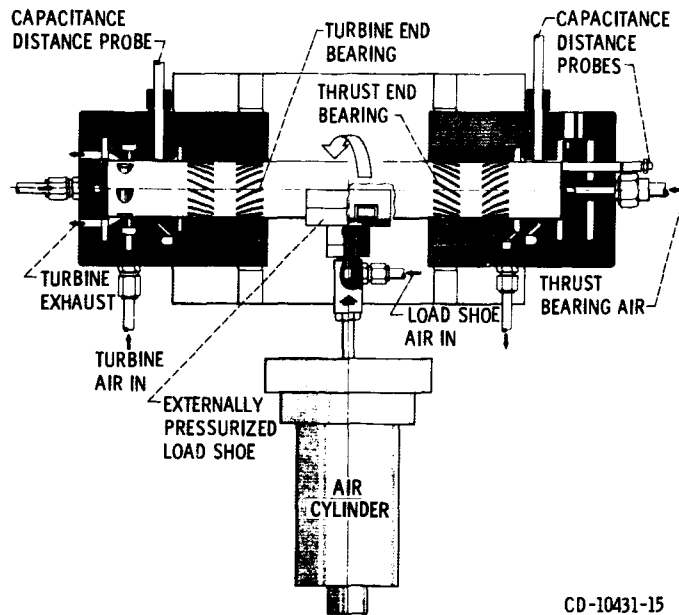
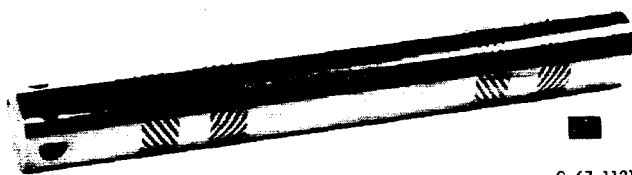
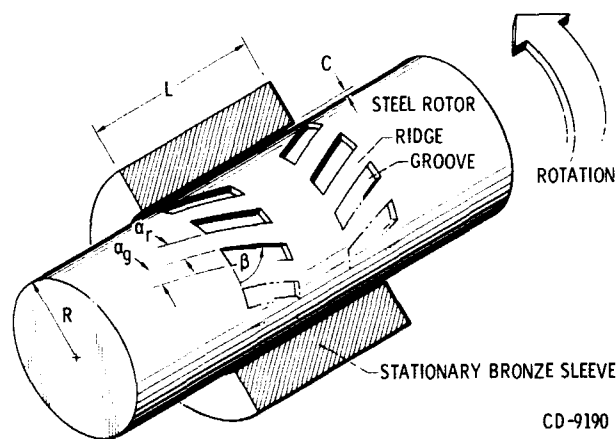


Figure 1. - Test apparatus.

CD-10431-15

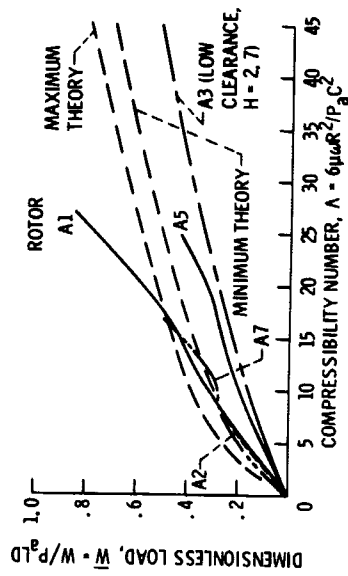


C-67-1121



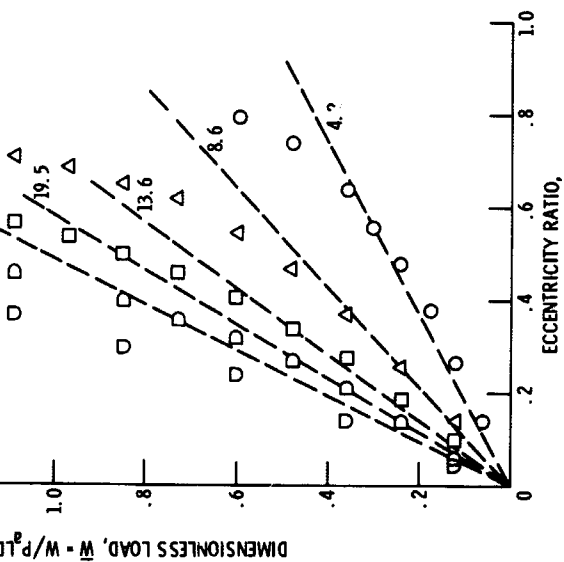
CD-9190

Figure 2. - Herringbone grooved rotor.



(a) Eccentricity ratio of 0.3.

Figure 4. - Experimental load capacity.



(b)  $\epsilon = 0.5$ .

Figure 4. - Concluded.

EXPERIMENTAL DATA  
 $\Lambda = 4.2$ ;  $N = 10\ 000$  RPM  
 $\Lambda = 8.6$ ;  $N = 20\ 000$  RPM  
 $\Lambda = 13.6$ ;  $N = 30\ 000$  RPM  
 $\Lambda = 19.5$ ;  $N = 40\ 000$  RPM  
 $\Lambda = 26.8$ ;  $N = 50\ 000$  RPM

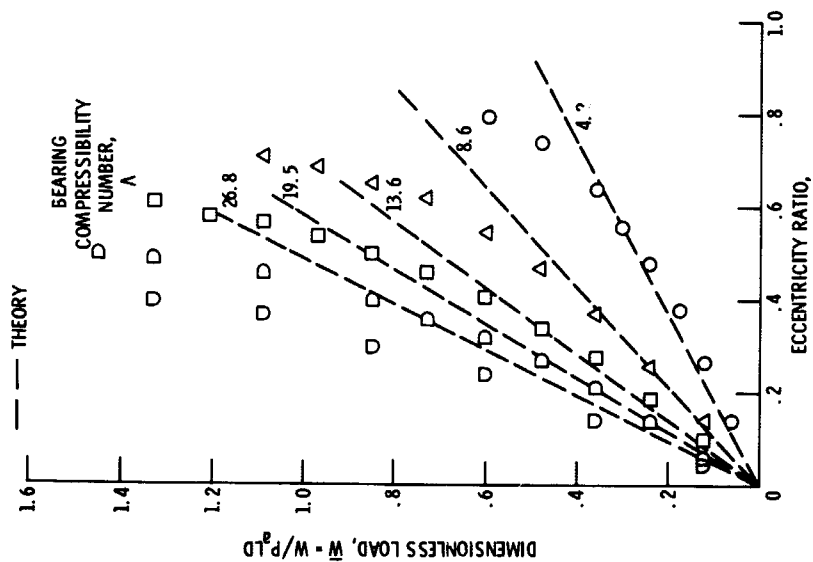


Figure 3. - Dimensionless load versus eccentricity ratio.

Rotor A-1 (turbine end bearing)  $\beta = 30^\circ$ ;  $\eta = 20$ ;  
 $\alpha = 0.5$ ;  $Y = 0.6$ ;  $H = 2.4$ ;  $C = 400$  microinches.

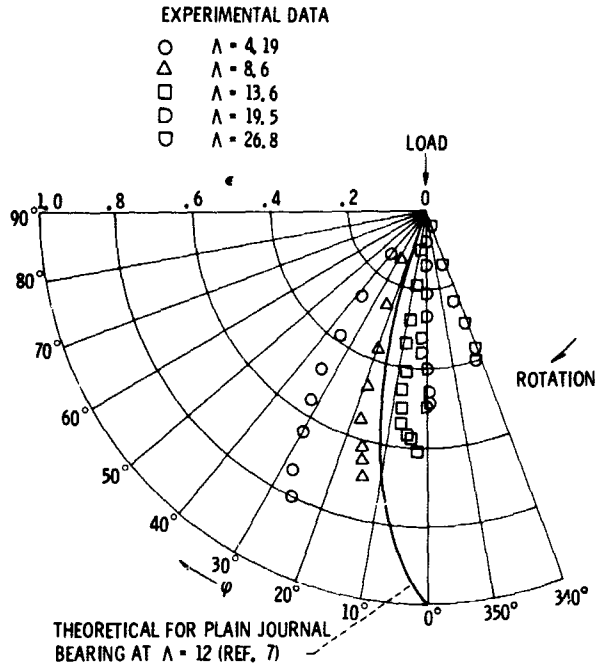


Figure 5. - Attitude angle versus eccentricity ratio for rotor A-1 (turbine end bearing).  $\beta = 30^\circ$ ;  $\eta = 20$ ;  $\alpha = 5$ ;  $L_1/L = 0.6$ ;  $L/D = 1$ ;  $H = 2.4$ ;  $C = 400$  microinches.

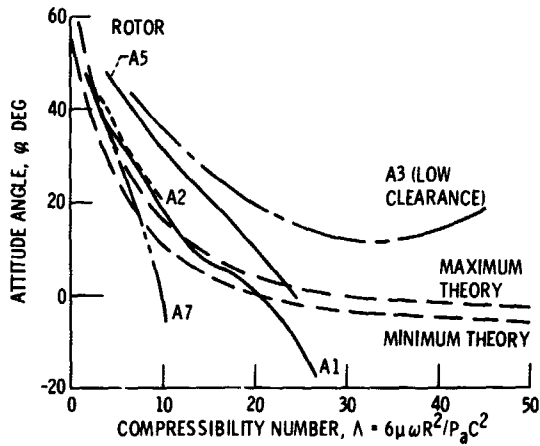


Figure 6. - Experimental attitude angles at eccentricity ratio of 0.3.

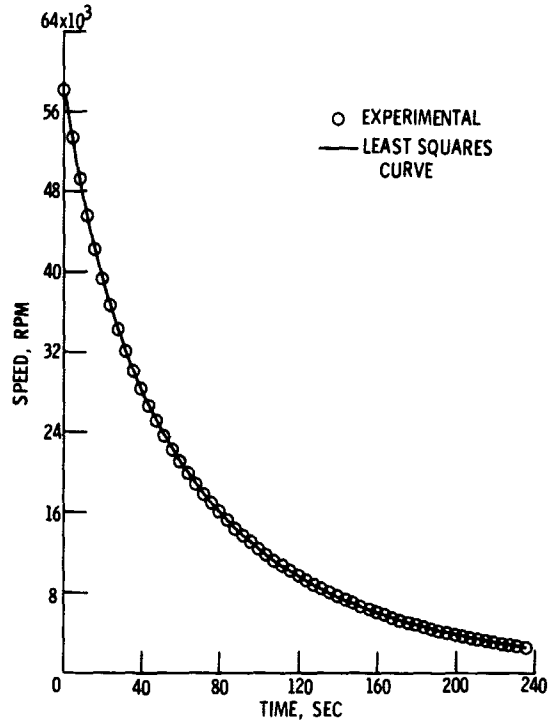


Figure 7. - Speed decay of herringbone-grooved bearing. Rotor A3; clearance, 420 microinches.

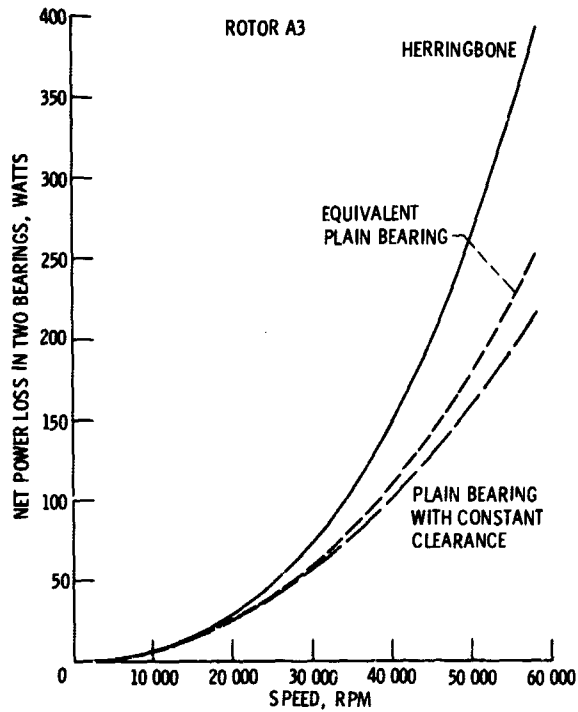


Figure 8. - Power loss of journal bearings.

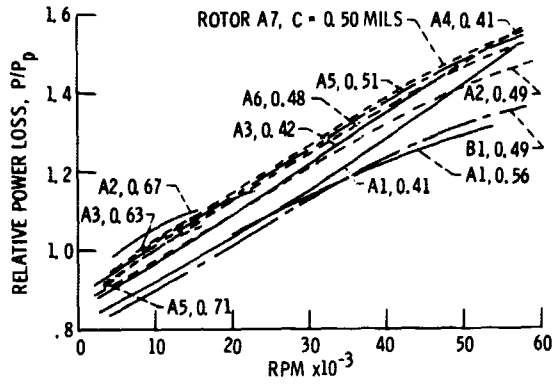


Figure 9. - Herringbone bearing power loss relative to plain journal bearing.

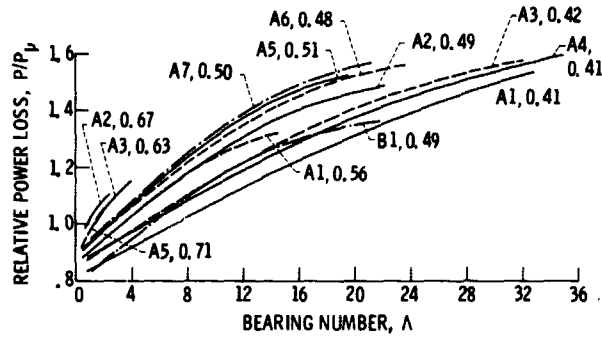


Figure 10. - Relative power loss versus bearing number.

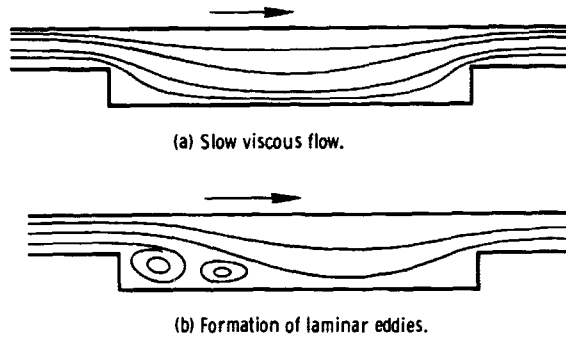


Figure 11. - Streamlines of flow in herringbone grooves.